



A chiral two-dimensional coordination polymer based on Cu^{II} and (*S*)-4,4'-bis(4-carboxyphenyl)-2,2'-bis(diphenylphosphinoyl)-1,1'-binaphthyl: Synthesis, structure, and magnetic and optical properties



Witri Wahyu Lestari^{a,1}, Peter Lönnecke^a, Huayna Cerqueira Streit^b, Frederik Schleife^a, Claudia Wickleder^{b,*}, Evamarie Hey-Hawkins^{a,*}

^a Institut für Anorganische Chemie, Fakultät für Chemie und Mineralogie, Universität Leipzig, Johannisallee 29, D-04103 Leipzig, Germany

^b Anorganische Chemie II, Fakultät IV, Department Chemie-Biologie, Universität Siegen, Adolf-Reichwein-Straße 2, D-57068 Siegen, Germany

ARTICLE INFO

Article history:

Received 16 March 2014

Received in revised form 30 May 2014

Accepted 10 June 2014

Available online 18 June 2014

Keywords:

Coordination polymers

Copper

BINAPO derivatives

Magnetic properties

Catalysis

Optical properties

ABSTRACT

The functionalized binaphthyl derivative (*S*)-4,4'-bis(4-carboxyphenyl)-2,2'-bis(diphenylphosphinoyl)-1,1'-binaphthyl (**H₂L**) was employed as linker in the synthesis of the chiral Cu^{II}-based two-dimensional network {[Cu₂(**L**)₂(dmf)₂·H₂O·9 dmf]_n (**1**). Single-crystal X-ray analysis showed a two-dimensional structure with a copper paddle wheel as secondary building unit. One dmf molecule is additionally axially coordinated to each Cu cation. A lamellar structure results consisting of alternating [Cu₂(**L**)₂(dmf)₂]_n and solvent (dmf, H₂O) layers. According to DTA/TG measurements the coordinated dmf molecules are released at about 320 °C, followed by decomposition around 460 °C. Magnetic susceptibility measurements on **1** indicate strong antiferromagnetic coupling between the two metal centers in Cu₂(**L**)₂(dmf)₂. Compound **1** exhibits ligand-based luminescence, assigned to the S₁ → S₀ transition of the aromatic units. Moreover, the emission spectrum of **1** is blueshifted in comparison to **H₂L**, due to different dihedral angles within the respective structures. Activated **1** (heating to 300 °C under vacuum for 3 h) showed low activity in the catalytic cyanosilylation of benzaldehyde (up to 27.1% conversion) and the isomerization of α-pinene oxide to campholenic aldehyde (up to 15.5% conversion).

© 2014 Elsevier B.V. All rights reserved.

1. Introduction

The design of multifunctional materials starting from the molecular level is an interesting research area and a great challenge, whereby the combination of organic, inorganic and technical chemistry plays a crucial role [1]. A relatively new class of hybrid organic–inorganic materials, constructed from metal atoms, cations, or clusters as nodes and bridging organic ligands as linkers to form infinitely extended metal–ligand networks, is one of the desired multifunctional material platforms. According to their porosity and dimensionality these networks can be classified as coordination polymers, porous coordination networks (PCNs), or porous coordination polymers (PCPs), also known as metal–organic

* Corresponding authors. Fax: +49 271 4702555 (C. Wickleder). Fax: +49 341 9739319 (E. Hey-Hawkins).

E-mail addresses: wickleder@chemie.uni-siegen.de (C. Wickleder), hey@rz.uni-leipzig.de (E. Hey-Hawkins).

¹ Present address: Department of Chemistry, The University of Sebelas Maret, Surakarta, Jawa Tengah 57126, Indonesia.

frameworks (MOFs) [2,3]. Compared to classical zeolite materials, the main advantage of the synthesis of coordination polymers or MOFs is the diverse design owing to a wide variety of organic linkers and metal nodes [4–6]. Thus, the linker design, that is, the choice of functional groups attached to the linker, chirality, rigidity and the coordinated metal ions, are important factors in the synthesis of coordination polymers and MOFs according to the proposed application [1a,7].

Coordination polymers and MOFs can exhibit useful magnetic [8] or luminescence [9] properties resulting from the combination of intrinsic properties of the metal center and the organic ligands [6]. Other specific properties, such as gas adsorption [10], molecular recognition or sensing [11], and catalytic activity [12], are additionally influenced by the structure itself, and this must be considered in the design process. However, thermal stability and stability of the framework after removal of guest molecules are a general problem [2,12c], and it is still a challenge to design stable porous MOFs with zeolite-type behavior for reversible exchange of guest molecules, especially for gas storage and catalysis [13]. In addition, weak interactions such as hydrogen bonding and π–π

stacking interactions are also important in the structural design of porous networks [14]

The majority of linkers employed are π -conjugated organic molecules with suitable rigid backbones functionalized with carboxylate or N-heterocyclic (e.g., pyridyl) moieties [1a,7]. The free organic ligands usually show emission (fluorescence) from the lowest excited singlet state to the singlet ground state, either $\pi \rightarrow \pi^*$ or $n \rightarrow \pi^*$ [9]. However, incorporation of these ligands as linkers in coordination polymers leads to reduction of the nonradiative decay rate and to increased fluorescence intensity, lifetimes, and quantum efficiencies [9]; thus, in general the spectra show shifted, broad emission bands and loss of fine structure compared to the free ligand. In the solid state, the close proximity facilitates molecular interactions. In coordination polymers based on non-emitting metal cations, factors that influence the ligand-based luminescence properties are, the orientation and the arrangement of the linkers (e.g., the dihedral angle between the aromatic rings), as well as the coordination environment within the network [9a].

Coordination polymers of transition metal ions with open shells such as Cu^{II} , Ni^{II} , or Co^{II} mostly quench the fluorescence generated from the organic linker [15]. However, there are exceptions such as $[\text{Ln}_2\text{Ni}(\text{Hbidc})_2(\text{SO}_4)_2(\text{H}_2\text{O})_8]_n$ ($\text{Ln} = \text{Pr}, \text{Sm}, \text{Eu}, \text{Gd}, \text{Tb}, \text{Dy}, \text{Ho}, \text{Er}, \text{Yb}$; $\text{H}_3\text{bidc} = 1H$ -benzimidazole-5,6-dicarboxylic acid), which show only partial quenching [16]. Even though luminescence quenching is initially considered a disadvantage, it is of crucial importance for the development of sensors, e.g., for oxygen sensing [17].

Coordination polymers or MOFs containing Cu^{II} cations or Cu clusters as nodes show a variety of coordination modes when constructing the secondary building unit (SBU) [5]: Cu_3 triangle [18], Cu_2 paddle wheel [19], Cu_4 rectangle [20] (distorted in the case of Cu^{I}) [21], and Cu_8 cube [22], Cu_2 paddle-wheel structures with four bridging carboxylato ligands based on modified phenyl [23], biphenyl [24], and binaphthyl [25] groups and other linkers have been reported [26]. Cu_2 paddle-wheel structures typically have additional weakly coordinating axial ligands such as water [23b,c,24,25] or strongly coordinating dmf [23a]. On removal, unsaturated Lewis acidic Cu centers are generated, and therefore these MOFs were mainly employed in catalysis [24,25,27]. Besides Cu_2 moieties based on Cu^{II} , M_2 or MM' paddle-wheel structures have also been observed with other metals [5], such as $\text{Ru}^{\text{II,III}}$ [28], Mo^{II} [29], Rh^{II} [30], Fe^{II} [31], Ni^{II} [32], Co^{II} [32], Cr^{II} [33], Zn^{II} [19b,31b,32b,34], Mn^{II} , W^{II} [35], Os^{III} [36], Cd^{II} [37], Bi^{II} [38], $\text{Bi}^{\text{II}}/\text{Rh}^{\text{II}}$ [39], Pt^{III} [40], Al^{III} [41], In^{III} [42], $\text{Pd}^{\text{II}}/\text{Co}^{\text{II}}$ [43], $\text{Pd}^{\text{II}}/\text{Mn}^{\text{II}}$ [43], $\text{Rh}^{\text{II}}/\text{Cu}^{\text{II}}$ [44], $\text{Rh}^{\text{II}}/\text{Zn}^{\text{II}}$ [44], $\text{Pd}^{\text{II}}/\text{Zn}^{\text{II}}$ [43], $\text{Mn}^{\text{II}}/\text{Zn}^{\text{II}}$ [45], $\text{Mn}^{\text{II}}/\text{Co}^{\text{II}}$ [45], $\text{Fe}^{\text{II}}/\text{Zn}^{\text{II}}$ [45], and $\text{Fe}^{\text{II}}/\text{Co}^{\text{II}}$ [45].

We here report the synthesis of the chiral Cu-based coordination polymer $\{[\text{Cu}_2(\text{L})_2(\text{dmf})_2] \cdot \text{H}_2\text{O} \cdot 9\text{dmf}\}_n$ (**1**) ($\text{L} = (S)$ -4,4'-bis(4-carboxylatophenyl)-2,2'-bis(diphenylphosphinoyl)-1,1'-binaphthyl) and its catalytic, magnetic and optical properties.

2. Experimental

2.1. Materials and general methods

Commercially available reagents were used as purchased. (*S*)-4,4'-bis(4-carboxyphenyl)-2,2'-bis(diphenylphosphinoyl)-1,1'-binaphthyl (**H₂L**) was prepared according to the literature procedure [46]. For catalytic tests, solvents were dried prior to use using standard procedures, and compound **1** was activated under vacuum (1×10^{-3} mbar, 300 °C, 3 h). The infrared spectra were recorded on a Perkin-Elmer System 2000 FTIR spectrometer by using KBr pellets in the range of 4000–400 cm^{-1} . Elemental analysis was performed with a Heraeus VARIO EL instrument CHN–O analyzer. Thermal analyses were performed on a NETZSCH STA/QMS system 409/429–403 thermal analyzer from room temperature to 900 °C

with a heating rate of 10 °C/min under helium atmosphere. The nitrogen adsorption isotherm at 77 K of **1** was obtained on an ASAP-2000 (Micromeritics) instrument equipped with a high-resolution pressure sensor. Prior to the isotherm measurements, the sample was heated at 100 °C for 12 h and then at 300 °C for 12 h. The magnetic susceptibility data were obtained in an external field of $B = 1$ T in the temperature range of 2–330 K with an MPMS 7XL SQUID magnetometer (Quantum Design).

2.2. Crystal structure determination

X-ray data were collected with a Gemini-S CCD diffractometer (Agilent Technologies) using MoK_α radiation ($\lambda = 0.71073$ Å) and omega scan rotation. Data collection and data reduction were done with CrysAlis Pro including the program SCALE3 ABSPACK for empirical absorption correction [47]. The structure of **1** was solved with Sir-92 [48]. Anisotropic refinement of all non-hydrogen atoms, except for non-coordinating solvent molecules (dmf), was performed with SHELXL-97 [49]. All hydrogen atoms were calculated on idealized positions. After several attempts to locate all solvent molecules, five extremely poorly defined dmf molecules were removed from the input file and the *hkl* file was corrected with the program SQUEEZE [50]. However, the SQUEEZE electron count of 91 electrons is related only to approximately 2.5 dmf molecules, i.e., half of the originally estimated number. The calculated volume of 292 Å³ for one of these dmf molecules appears to be much too large. The reported and expected volume for one dmf molecule is 102 Å³ [51]. For this reason, the originally detected five extremely poorly defined dmf molecules were used to calculate the formula, $F(000)$, and all other composition-dependent parameters of the compound. The calculated molecular volume of 146 Å³ for the dmf molecules is much closer to the expected value. Structure figures were generated with Diamond-3 [52].

Crystallographic data for $\{[\text{Cu}_2(\text{L})_2(\text{dmf})_2] \cdot \text{H}_2\text{O} \cdot 9\text{dmf}\}_n$ (**1**): $\text{C}_{149}\text{H}_{155}\text{Cu}_2\text{N}_{11}\text{O}_{24}\text{P}_4$, $M = 2734.80$, triclinic, space group $P1$, $a = 10.1470(4)$, $b = 19.2737(7)$, $c = 19.5457(7)$ Å, $\alpha = 101.853(3)^\circ$, $\beta = 100.137(3)^\circ$, $\gamma = 103.590(3)^\circ$, $V = 3533.8(2)$ Å³, $Z = 1$, $\rho_{\text{calcd}} = 1.285$ Mg m^{-3} , $\mu(\text{MoK}_\alpha) = 0.419$ mm^{-1} . Least-squares refinement based on 45370 collected (24883 independent) reflections and 1505 parameters led to convergence, with a final $R_1 = 0.0520$ ($I > 2\sigma(I)$), $wR_2 = 0.1313$ ($I > 2\sigma(I)$), Flack parameter = 0.016(8), and GOF = 1.015. The crystal data can be obtained free of charge from The Cambridge Crystallographic Data Centre via www.ccdc.cam.ac.uk/data_request/cif (CCDC number 958437).

The X-ray powder diffraction (PXRD) measurements were carried out on a STOE STADI P diffractometer in the Debye–Scherrer mode using $\text{CuK}_{\alpha 1}$ radiation ($\lambda = 1.5406$ Å). The samples for these measurements were prepared in glass capillaries (outer diameter 0.5 mm).

2.3. Synthesis of $\{[\text{Cu}_2(\text{L})_2(\text{dmf})_2] \cdot \text{H}_2\text{O} \cdot 9\text{dmf}\}_n$ (**1**)

Solvothermal synthesis of **1** was carried out in stainless steel autoclaves with Teflon liner (Parr). The temperature programs were applied in an oven ULE400 (Memmert) using the software Celsius 2005 (Version 6.1). A mixture of dmf/ H_2O (3 mL/1 mL) was added to **H₂L** (20 mg, 0.022 mmol) and $\text{Cu}(\text{NO}_3)_2 \cdot 3\text{H}_2\text{O}$ (20 mg, 0.083 mmol) in a 15 mL Teflon-lined autoclave. After addition of 3 drops of HCl (3 M, aq.) or 1 drop of concentrated HCl (67%), the vial was capped and placed in an oven at 90 °C for three days, followed by a cooling time of 72 h. Prismatic blue-green crystals (20 mg, 33%) were obtained, isolated by filtration, and dried at room temperature. Scale up was performed by using two 200 mL PARR reactors: $\text{Cu}(\text{NO}_3)_2 \cdot 3\text{H}_2\text{O}$ (0.4 g, 1.66 mmol) and **H₂L** (0.4 g, 0.45 mmol) in dmf (60 mL), water (20 mL) and 20 drops of concentrated HCl. Yield: 0.52 g, 42.3% (based on **H₂L**). Anal. Calc. for **1** (%):

$C_{149}H_{155}Cu_2N_{11}O_{24}P_4$ (2734.80): C, 65.44; H, 5.71; N, 5.63; O, 14.04. Found: C, 64.54; H, 5.21; N, 3.99; O, 15.98%. (indicates loss of dmf and uptake of water). IR (KBr pellet, cm^{-1}): 3448 (br, OH, H bonding), 3056 (m), 2929 (m, C–H), 2346 (w), 1665 (s, $\nu_{as}COO$), 1621 (s, CO, dmf), 1545 (w, ν_sCOO), 1499 (m), 1437 (s, P–C₆H₅), 1403 (s), 1257 (m), 1196 (s, $\nu_{as}P=O$), 1101 (s, $\nu_sP=O$), 1020 (m), 975 (s), 866 (s), 833 (w), 789 (s), 752 (s, C–H), 722 (s), 698 (m, P–C), 666 (m), 592 (w), 546 (s, C–H). After heating at 250 °C under vacuum for 3 h: 3410 (br, OH, H bonding), 3054 (m), 1608 (s, $\nu_{as}COO$), 1539 (s, ν_sCOO), 1436 (s, P–C₆H₅), 1400 (s), 1181 (s, $\nu_{as}P=O$), 1115 (s, $\nu_sP=O$), 1019 (s), 999 (m), 974 (s), 864 (s), 787 (s, C–H), 751 (w), 722 (s), 693 (s, P–C), 592 (m), 546 (s, C–H).

2.4. Catalytic tests

All reactions were performed in schlenks.

2.4.1. General procedure for cyanosilylation of benzaldehyde

0.1 g (5 mol-%) of activated **1** was transferred to a reaction vessel, and solvent (10 ml, see Table 1) and reactants (trimethylsilyl cyanide, 0.25 ml, 2.0 mmol, Alfa Aesar, 98%; benzaldehyde, 0.1 ml, 1 mmol, Alfa Aesar, distilled, 99.9%) were added. The suspension was stirred for 48 h at various temperatures (see Table 1) and the products were analyzed after filtration with GC/MS.

2.4.2. General procedure for isomerization of α -pinene oxide to campholenic aldehyde

0.031 g (10 mol-%) of activated **1** was transferred to a reaction vessel, and solvent (5 ml, see Table 1) and α -pinene oxide (0.026 ml, 0.164 mmol, ABCR) were added. The suspension was stirred for 72 h at room temperature. After filtration the products were analyzed with GC/MS. For comparison, the reaction was carried out without the catalyst in MeOH.

2.5. Luminescence measurements

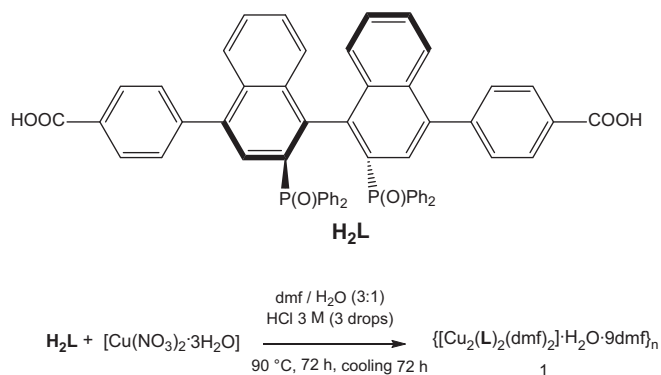
Photoluminescence investigations at room and low temperature on solid samples sealed in silica ampoules were carried out with a Jobin Yvon fluorescence spectrometer (Fluorolog 3) equipped with two 0.22 m double monochromators (SPEX, 1680) and a 450 W xenon lamp. Cooling to 10 K was achieved by a closed-cycle He cryostat (Janis Research). The emission spectra were corrected for photomultiplier sensitivity, the excitation spectra for lamp intensity, and both for the transmission of the monochromators. For reflection measurements in the UV–Vis range, a Cary 5000 (Varian) was used.

3. Results and discussion

The Cu^{II}-based coordination polymer $\{[Cu_2(L)_2(dmf)_2] \cdot H_2O \cdot 9 dmf\}_n$ (**1**) was obtained as blue-green prismatic crystals from copper(II) nitrate and **H₂L** [46] under solvothermal conditions in dmf/H₂O (3/1 mL) in the presence of 3 drops of HCl (3 M) at 90 °C for 3 d (Scheme 1). Compound **1** crystallizes in the triclinic space group *P1* with one molecule in the unit cell.

3.1. Solid-state structure

In **1**, two Cu^{II} cations are bridged by four dianionic linkers (**L**²⁻) (Cu(1)–Cu(2) 2.64 Å), each with one carboxylate group coordinated in an $\mu_2:\eta^1,\eta^1$ fashion (*syn-syn* mode) to generate a paddle-wheel structure (Fig. 1) with O–Cu–O bond angles around 90°, Cu–O_{carboxylate} bond lengths ranging from 1.95(3) to



Scheme 1. Synthesis of **1**.

2.00(3) Å, and O–C–O bond angles from 123.7(4) to 127.5(4)°. Additional coordination of each Cu^{II} cation by one dmf molecule (Cu–O 2.17 Å) results in a square-pyramidal coordination environment. The bridging dianionic ligands connect the Cu₂ units into a two-dimensional (111)-oriented layer structure (Fig. 2) with a pore size of about 12 × 14 Å² (calculated with Diamond [52]). The dihedral angles between the naphthyl rings in the linkers of compound **1** (82.99(9) to 85.0(1)°) and between the naphthyl and phenyl rings (46.0(1) to 60.2(2)°) are slightly larger than the dihedral angles in **H₂L** (82.1(3)° and 44.1(5)°, respectively) [46]. The framework shows *sql* topology (4-c net), with point (Schläfli) symbol {4⁴.6²} according to TOPOS [53] and the RCSR database [54].

Weak interactions such as hydrogen bonding and π – π stacking interactions play an important role in the architecture of coordination networks. In **1**, the two-dimensional sheets are connected by weak π – π stacking interactions, similar to those observed in $[Cu\{1,4-(COO)_2C_6H_4\}(dmf)]_n$ [23a] and $[Zn\{1,4-(COO)_2C_6H_4\}(H_2O)(dmf)]_n$ (MOF-2) [34a].

Additionally, hydrogen bonds are observed between a water molecule (one per formula unit) and P=O groups of two neighboring layers (Fig. S1, ESI). The framework of **1** is further stabilized by solvent molecules (9 dmf per formula unit), which occupy the cavities.

A total potential solvent-accessible void volume of 3510.5 Å³ (21.9%) per unit cell was calculated with PLATON [50,55]. However, after thermal treatment, measurement of the nitrogen adsorption isotherm showed only very small micropores (0.0009 cm³/g with a surface area of ca. 4 m²/g after heating at 100 °C for 12 h, and 12 m²/g after heating at 300 °C for 12 h). This surface area is seven times higher than that of the previously reported Cu^{II}-based MOF with a 5,5'-dicarboxylate-modified BINOL ligand, $\{[Cu_2(5,5'-BDA)_2(H_2O)_2] \cdot MeOH \cdot 2 H_2O\}$ (BDA = 2,2'-dihydroxy-1,1'-binaphthalene-5,5'-dicarboxylate) (1.71 m²/g) [25a]. This indicates removal of solvent molecules and collapse of the framework of **1** on heating. This was also supported by powder X-ray diffraction on wet and dry samples (see ESI, Fig. S2). Therefore, **1** is only potentially useful as a heterogeneous catalyst based on surface-activity, as was reported by Tanaka et al. for similar compounds, $\{[Cu_2(5,5'-BDA)_2(H_2O)_2] \cdot MeOH \cdot 2 H_2O\}$ [25a] but not based on porosity.

The thermogravimetric profile shows loss of dmf up to about 220 °C (weight loss of 16.3%; calcd 16.7% for loss of 6 dmf and 1 H₂O; see ESI, Fig. S3). In the temperature range of 220 to 300 °C, loss of the two coordinated dmf molecules was observed (5.6%; calcd 5.4%). Complete decomposition started at about 460 °C and resulted in face-centered cubic CuO as final product (verified by temperature-programmed X-ray powder diffraction, according to ICSD [56]; see ESI, Fig. S4). In the IR spectrum, absorption bands for the Cu(L) fragment and dmf are observed; the CO stretching

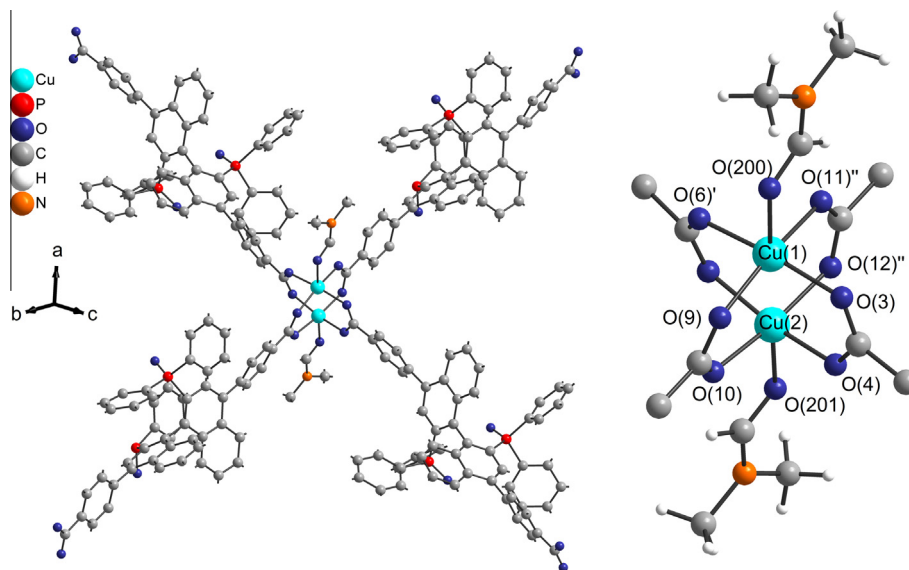


Fig. 1. Section of $[\text{Cu}_2\text{L}_2(\text{dmf})_2]_n$ (left) and paddle-wheel SBU (right). Symmetry transformation used to generate equivalent atoms ($'$): $x + 1, y, z - 1$; ($''$): $x + 1, y - 1, z$.

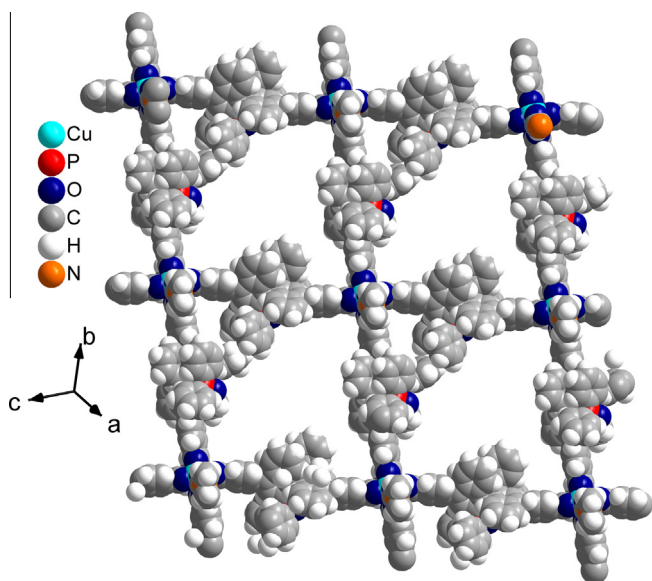


Fig. 2. Two-dimensional network of $[(\text{Cu}_2(\text{L})_2(\text{dmf})_2) \cdot \text{H}_2\text{O} \cdot 0.9 \text{ dmf}]_n$ (**1**), pore size $12 \times 14 \text{ \AA}^2$ (in space-filling mode, Diamond [52]).

vibration of coordinated dmf is shifted to lower wavenumbers (1621 cm^{-1}) compared to free dmf (1676 cm^{-1}). After heating at $250 \text{ }^\circ\text{C}$ under vacuum for 3 h, only vibrations for Cu(L) are visible. Removal of dmf results in a shift of the $\nu_{\text{as}}(\text{COO})$ band from 1665 cm^{-1} (in **1**) to 1608 cm^{-1} and of the $\nu_{\text{s}}(\text{COO})$ band from 1545 cm^{-1} (in **1**) to 1539 cm^{-1} .

For removal of the coordinated dmf molecules to obtain a catalytically active species, **1** was heated at $300\text{--}320 \text{ }^\circ\text{C}$ under vacuum for 3 h. As an alternative, solvent exchange with methanol by soxhlet extraction was also conducted. However, both methods resulted in poor crystallinity, as shown by powder X-ray diffraction (see ESI, Fig. S2). This indicates that methanol does not coordinate to copper(II) in the same way as dmf.

3.2. Preliminary catalytic tests

Compound **1** was activated by heating to $300 \text{ }^\circ\text{C}$ under vacuum for 3 h and its catalytic activity tested in the cyanosilylation of

benzaldehyde and the isomerization of α -pinene oxide to campholenic aldehyde (Table 1).

The activity of the catalyst is rather low indicating incomplete loss of coordinated dmf at the temperatures employed. However, at higher temperatures, decomposition of **1** occurs.

Table 1
Cyanosilylation of benzaldehyde and isomerization of α -pinene oxide to campholenic aldehyde with activated **1** as catalyst.

Substrate	Solvent	Temperature/time	Yield (%)
Benzaldehyde	CH_2Cl_2	$40 \text{ }^\circ\text{C}/48 \text{ h}$	12.2
Benzaldehyde	Toluene	$80 \text{ }^\circ\text{C}/48 \text{ h}$	24.2
Benzaldehyde	<i>n</i> -Pentane	$40 \text{ }^\circ\text{C}/48 \text{ h}$	27.1
α -Pinene oxide	$\text{C}_2\text{H}_4\text{Cl}_2$	RT/72 h	2.3
α -Pinene oxide	Ethyl acetate	RT/72 h	7.9
α -Pinene oxide	Methanol	RT/72 h	15.5
α -Pinene oxide (no catalyst)	Methanol	RT/72 h	0.4

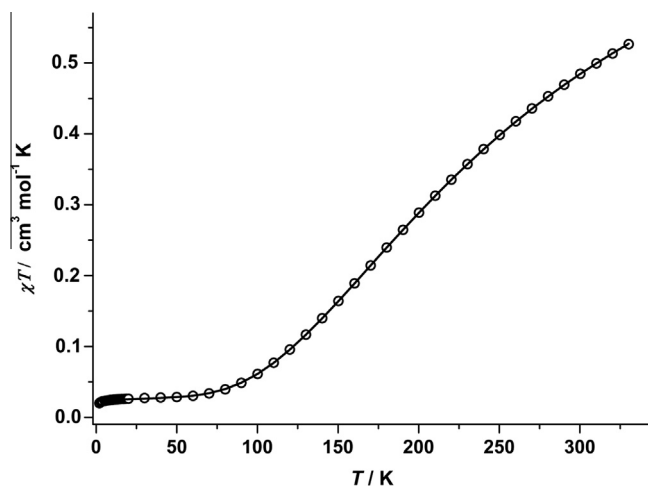


Fig. 3. Temperature-dependence of $\chi_{\text{M}}T$ for **1** (per dinuclear unit). The open circles represent the experimental values and the solid line the best theoretical fit according to Eq. (1).

3.3. Magnetic properties

The temperature-dependent magnetic susceptibility of compound **1** (Fig. 3) indicates strong intramolecular antiferromagnetic exchange coupling between the two Cu^{II} centers, as the χ_{MT} value steadily decreases from 0.53 cm³ mol⁻¹ K at 330 K to 0.03 cm³ mol⁻¹ K at 70 K and then decreases slightly to 0.02 cm³ mol⁻¹ K at 2 K.

The temperature dependence of **1** was simulated by using the appropriate spin Hamiltonian [Eq. (1)] [57], containing the isotropic Heisenberg–Dirac–van Vleck (HDvV) exchange and a Zeeman interaction, by using a full-matrix diagonalization approach [58], assuming identical *g* values for the two Cu ions.

$$\hat{H} = -2J\hat{S}_1\hat{S}_2 + \sum_{i=1}^2 g_i\mu_B\hat{S}_{i\tau}B_{\tau}(\tau = x, y, z) \quad (1)$$

By taking into account the temperature-independent paramagnetism (TIP) [59] and a small amount (6.2%) of a paramagnetic impurity of uncoupled paramagnetic ions (*S* = 1/2), a good fit over the whole temperature range was possible, yielding *J* = −166.3 cm⁻¹, *g* = 2.20, and TIP = 1.07 × 10⁻⁴ cm³ mol⁻¹. The paramagnetic impurity was included with a routine implemented in the MagProp software package [58]. The *J* and *g* values are in good agreement with values reported for related dinuclear Cu^{II} complexes [23a,60].

3.4. Optical properties

Reflection measurements on **1** (Fig. 4) showed a continuous increase for energies higher than 14000 cm⁻¹, with a maximum at approximately 20000 cm⁻¹, followed by a constant decrease up to 28000 cm⁻¹. The reflection distributed over the blue-green spectral range correlates with the color (blue-green) of the crystals (Fig. 4, inset). The absorbance in the low-energy range can be attributed to Cu²⁺ ions exclusively, because the ligands do not show any absorption in this range (see Fig. 6b below), while the absorption at high energies can be attributed to both Cu²⁺ and ligand. In general, inorganic Cu^{II} complexes show a green color with a strong Jahn–Teller effect for square-planar coordination, while the color shifts to blue if the Jahn–Teller distortion is not strong, that is, elongated octahedral coordination [61]. In fact, our observations agree with these general observations due to the square-pyramidal coordination of **1**.

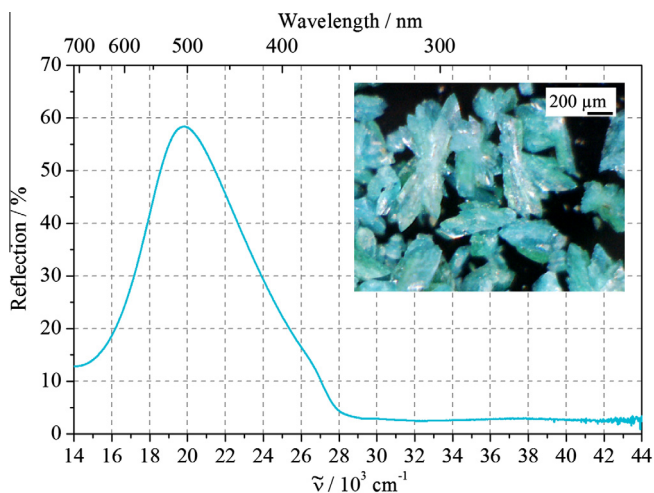


Fig. 4. Reflection spectrum of **1**. Inset: blue-green crystals of **1** in daylight. (For interpretation of the references to color in this figure legend, the reader is referred to the web version of this article.)

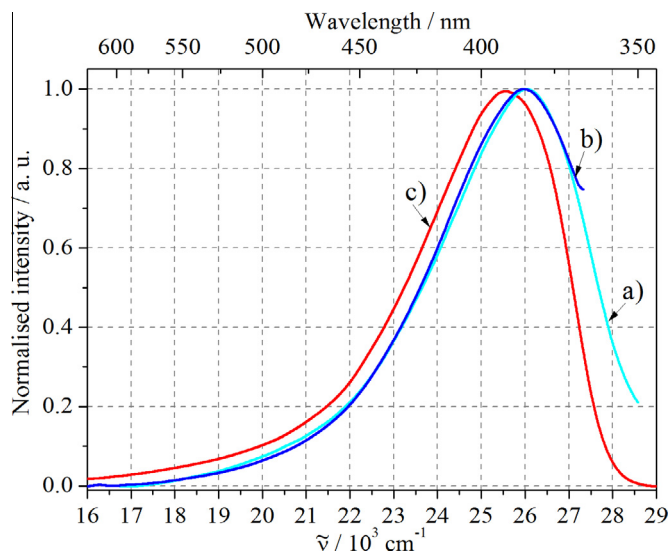


Fig. 5. Emission spectra of **1** excited at a) $\tilde{\nu}_{\text{ex}} = 30769 \text{ cm}^{-1}$ (in light blue), and b) $\tilde{\nu}_{\text{ex}} = 28902 \text{ cm}^{-1}$ (in dark blue). c) Emission spectrum of **H₂L** (excited at $\tilde{\nu}_{\text{ex}} = 25574 \text{ cm}^{-1}$, in red). (For interpretation of the references to color in this figure legend, the reader is referred to the web version of this article.)

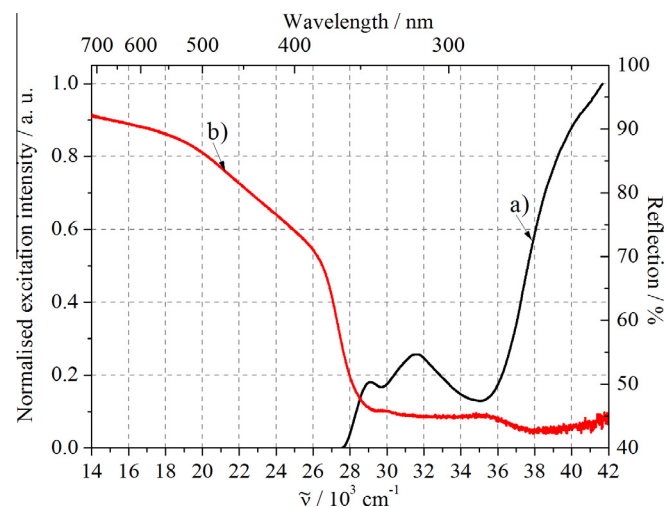


Fig. 6. a) Excitation spectrum of **1** ($\tilde{\nu}_{\text{ex}} = 25773 \text{ cm}^{-1}$, in black) in comparison to b) the reflection spectrum of **H₂L** (in red). (For interpretation of the references to color in this figure legend, the reader is referred to the web version of this article.)

The solid-state emission spectra of **1** at room temperature (Fig. 5) consist of a nearly Gaussian curve with a maximum at 25 773 cm⁻¹, invariable in position and shape for different excitation energies, for example, 30 769 cm⁻¹ (Fig. 5a, in light blue) and 28 902 cm⁻¹ (Fig. 5b, in dark blue).

Similar to **1**, the emission spectrum of **H₂L** (Fig. 5c, in red) consists of a nearly Gaussian shaped band, centered at 25 581 cm⁻¹ ($\tilde{\nu}_{\text{ex}} = 25 574 \text{ cm}^{-1}$) [62]. This band can be assigned to the *S*₁ → *S*₀ transitions of the aromatic units, as shown previously [62]. The similarity in shape and position of the emission spectra of **1** and **H₂L** suggest that this phenomenon is ligand-based luminescence. This statement is supported by the fact that Cu^{II} in general does not show any luminescence but quenching [63]. The shifts of the positions of the luminescence bands can be explained by the different dihedral angles of the aromatic rings within the structures of **1** and **H₂L** [64]. In general, a smaller dihedral angle results in enhanced interactions of the π electrons, shifting the emission bands to lower energies. Since, in this case, the dihedral angles in

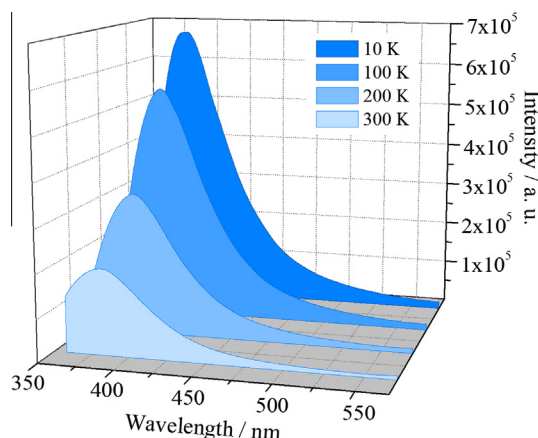


Fig. 7. Effect of decreasing temperatures on the emission spectrum ($\bar{\nu}_{\text{ex}} = 31348 \text{ cm}^{-1}$) of **1**.

H₂L are slightly smaller than in **1**, the blueshift observed in the emission spectrum of **1** ($\Delta E = 152 \text{ cm}^{-1}$) in comparison to **H₂L** is expected. This observation is in contrast to the redshift that was observed for the ligand-based emission bands of $\{[\text{Na}_2\text{Pb}_2(\text{L}')_3(\text{H}_2\text{O})(\text{dmf})_4] \cdot 9 \text{ dmf}\}_n$ [65] ($\text{L}' = (\text{S})$ -5,5'-bis(4-carboxyphenyl)-2,2'-bis(diphenylphosphinoyl)-1,1'-binaphthyl) and $\{[\text{Cd}_2(\text{L})_2(\text{H}_2\text{O})] \cdot 18 \text{ dmf}\}_n$ [62] compared to **H₂L** (or **H₂L'**). Although the dihedral angles in the excited states are unknown, it can be assumed that the conformations will not change remarkably during the excitation processes, due to the packing forces in the rigid crystal structures.

Comparing Figs. 4 and 5 reveals an overlap of the spectral ranges of absorption and emission of **1**. Thus, a significant Cu^{II}-assisted absorbance of the ligand emission explains the strong quenching effect of the emission of **1** in comparison to the emission properties of **H₂L**. As reported previously [62], the quantum yield of **H₂L** is 33%, whereas the emission of **1** is too weak to be determined.

A further indication for the assignment of the optical properties of **1** as ligand-based luminescence is the similarity between the excitation spectrum of **1** ($\bar{\nu}_{\text{em}} = 25\,773 \text{ cm}^{-1}$, Fig. 6a, in black) and the reflection spectrum of **H₂L** (Fig. 6b, in red). This figure displays a decrease of the reflection intensity of **H₂L** for energies larger than $20\,000 \text{ cm}^{-1}$, more pronounced for energies higher than $26\,000 \text{ cm}^{-1}$, indicating an increase of the absorption in this spectral region. Furthermore, the reflection spectrum shows the formation of two main absorption bands: one between about $26\,000$ and $28\,000 \text{ cm}^{-1}$ as well as another band between $28\,000$ and $36\,000 \text{ cm}^{-1}$. An analogous trend is observed for the excitation spectrum of **1**, which rises at $27\,500 \text{ cm}^{-1}$ and increases starting at $36\,000 \text{ cm}^{-1}$.

Luminescence measurements at very low temperatures, e.g., 10 K, are important for studying possible additional transitions, which may be quenched at room temperature. The emission spectra of **1** at 10 K and at room temperature (Fig. 7) are very similar in shape and position, and thus indicate no additional transitions in this energy range. However, the emission intensity is 70% higher at 10 K than at room temperature. This behavior is explained by energy loss by nonradiative vibronic-assisted transitions with increasing temperature.

4. Conclusion

The homochiral two-dimensional coordination polymer $\{[\text{Cu}_2(\text{L})_2(\text{dmf})_2] \cdot \text{H}_2\text{O} \cdot 9 \text{ dmf}\}_n$ (**1**) is based on a paddle-wheel SBU with strong antiferromagnetic exchange coupling between the

two Cu^{II} centers. Compound **1** exhibits ligand-based luminescence, assigned to the $\text{S}_1 \rightarrow \text{S}_0$ transition of the aromatic units. The emission spectrum of **1** is blueshifted in comparison to **H₂L**, due to differences in the dihedral angles within the respective structures.

Acknowledgments

This work was supported by FFTF (Faculty for the Future) Schlumberger Foundation for Women in Science and Engineering (doctoral fellowship for W.W.L.). We thank M.Sc. Marcel Handke, Leipzig University, for powder X-ray measurement and TOPOS analysis, and Prof. Wolf-Dietrich Einicke, Leipzig University, for nitrogen adsorption and BET surface area measurement.

Appendix A. Supplementary material

Supplementary data (hydrogen bonding in compound **1**, powder X-ray diffraction of compound **1**, thermogravimetry analysis of compound **1**, temperature-dependent powder X-ray diffraction and IR data for compound **1** after solvent exchange with methanol) associated with this article can be found, in the online version, at <http://dx.doi.org/10.1016/j.ica.2014.06.006>. These data include MOL files and InChIKeys of the most important compounds described in this article.

References

- [1] (a) L. MacGillivray, *Metal–Organic Frameworks: Design and Application*, Wiley, Hoboken, New Jersey, 2010; (b) H.-C. Zhou, J.R. Long, O.M. Yaghi, *Chem. Rev.* 112 (2012) 673.
- [2] C. Janiak, J.K. Vieth, *New J. Chem.* 34 (2010) 2366.
- [3] S.R. Batten, N.R. Champness, X.-M. Chen, J.G. Martinez, S. Kitagawa, L. Öhrström, M. O’Keeffe, M.P. Suh, J. Reedijk, *CrystEngComm* 14 (2012) 3001.
- [4] M. O’Keeffe, *Chem. Soc. Rev.* 38 (2009) 1215.
- [5] D.J. Tranchemontagne, J.L. Mendoza-Cortés, M. O’Keeffe, O.M. Yaghi, *Chem. Soc. Rev.* 38 (2009) 1257.
- [6] J.J. Perry IV, J.A. Perman, M.J. Zaworotko, *Chem. Soc. Rev.* 38 (2009) 1400.
- [7] (a) O.M. Yaghi, M. O’Keeffe, N.W. Ockwig, H.K. Chae, M. Eddaoudi, J. Kim, *Nature* 423 (2003) 705; (b) D. Farrusseng, *Metal–Organic Frameworks: Applications from Catalysis to Gas Storage*, Wiley-VCH, Weinheim, Germany, 2011.
- [8] (a) E. Coronado, G.M. Espallargas, *Chem. Soc. Rev.* 42 (2013) 1525; (b) M. Kurmoo, *Chem. Soc. Rev.* 38 (2009) 1353.
- [9] (a) Y. Cui, Y. Yue, G. Qian, B. Chen, *Chem. Rev.* 112 (2012) 1126; (b) M.D. Allendorf, C.A. Bauer, R.K. Bhakta, R.J.T. Houk, *Chem. Soc. Rev.* 38 (2009) 1330.
- [10] (a) H. Wu, Q. Gong, D.H. Olson, J. Li, *Chem. Rev.* 112 (2012) 836; (b) J.-R. Li, R.J. Kuppler, H.-C. Zhou, *Chem. Soc. Rev.* 38 (2009) 1477.
- [11] (a) L.E. Kreno, K. Leong, O.K. Farha, M. Allendorf, R.P.V. Duyne, J.T. Hupp, *Chem. Rev.* 112 (2012) 1105; (b) C. Valente, E. Choi, M.E. Belowich, C.J. Doonan, Q. Li, T.B. Gasa, Y.Y. Botros, O.M. Yaghi, J.F. Stoddart, *Chem. Commun.* 46 (2010) 4911; (c) B. Chen, S. Xiang, G. Qian, *Acc. Chem. Res.* 43 (2010) 1115.
- [12] (a) J.Y. Lee, O.K. Farha, J. Roberts, K.A. Scheidt, S.T. Nguyen, J.T. Hupp, *Chem. Soc. Rev.* 38 (2009) 1450; (b) L. Ma, C. Abney, W. Lin, *Chem. Soc. Rev.* 38 (2009) 1248; (c) W. Lin, *Top. Catal.* 53 (2010) 869; (d) M. Yoon, R. Srirambalaji, K. Kim, *Chem. Rev.* 112 (2012) 1196.
- [13] S.K. Ghosh, S. Kitagawa, *CrystEngComm* 10 (2008) 1739.
- [14] S. Kitagawa, R. Kitaura, S. Noro, *Angew. Chem.* 116 (2004) 2388 (*Angew. Chem., Int. Ed.* 43 (2004) 2334).
- [15] (a) A. Vogler, H. Kunkely, in: H. Yersin (Ed.), *Transition Metal and Rare Earth Compounds*, Springer, Berlin, 2001, p. 183; (b) J. Heine, K. Müller-Buschbaum, *Chem. Soc. Rev.* 42 (2013) 9232.
- [16] Y.-G. Sun, G. Xiong, M.-Y. Guo, F. Ding, S.-J. Wang, P.F. Smet, D. Poelman, E.-J. Gao, F. Verpoort, *Dalton Trans.* 41 (2012) 7670.
- [17] Z. Xie, L. Ma, K.E. deKrafft, A. Jin, W. Lin, *J. Am. Chem. Soc.* 132 (2010) 922.
- [18] G. Mezei, M. Rivera-Carrillo, R.G. Raptis, *Inorg. Chim. Acta* 357 (2004) 3721.
- [19] (a) P. Drożdżewski, A. Brożyna, M. Kubiak, *J. Mol. Struct.* 707 (2004) 131; (b) B. Moulton, H. Abourahma, M.W. Bradner, J. Lu, G.J. McManus, M.J. Zaworotko, *Chem. Commun.* (2003) 1342.
- [20] P. Knuutila, *Inorg. Chim. Acta* 58 (1982) 201.
- [21] D.L. Reger, M.F. Huff, T.A. Wolfe, R.D. Adams, *Organometallics* 8 (1989) 848.
- [22] G.A. Ardizzoia, M.A. Angaroni, G.L. Monica, F. Cariati, M. Moret, N. Masciocchi, *J. Chem. Soc., Chem. Commun.* (1990) 1021.
- [23] (a) C.G. Carson, K. Hardcastle, J. Schwartz, X. Liu, C. Hoffmann, R.A. Gerhardt, R. Tannenbaum, *Eur. J. Inorg. Chem.* (2009) 2338; (b) S.S.-Y. Chui, S.M.-F. Lo, J.P.H. Charmant, A.G. Orpen, I.D. Williams, *Science*

- 283 (1999) 1148;
(c) L. Gao, B. Zhao, G. Li, Z. Shi, S. Feng, *Inorg. Chem. Commun.* 6 (2003) 1249.
- [24] (a) K.S. Jeong, Y.B. Go, S.M. Shin, S.J. Lee, J. Kim, O.M. Yaghi, N. Jeong, *Chem. Sci.* 2 (2011) 877;
(b) X.-Z. Wang, D.-R. Zhu, Y. Xu, J. Yang, X. Shen, J. Zhou, N. Fei, X.-K. Ke, L.-M. Peng, *Cryst. Growth Des.* 10 (2010) 887;
(c) L. Ma, *Inorg. Chem.* 47 (2008) 3955.
- [25] (a) K. Tanaka, S. Oda, M. Shiro, *Chem. Commun.* (2008) 820;
(b) L. Ma, D.J. Mihalcik, W. Lin, *J. Am. Chem. Soc.* 131 (2009) 4610;
(c) L. Ma, J.M. Falkowski, C. Abney, W. Lin, *Nat. Chem.* 2 (2010) 838;
(d) L. Ma, W. Lin, *J. Am. Chem. Soc.* 130 (2008) 13834.
- [26] M. Köberl, M. Cokoja, W.A. Herrmann, F.E. Kühn, *Dalton Trans.* 40 (2011) 6834.
- [27] (a) K. Schlichte, T. Kratzke, S. Kaskel, *Micropor. Mesopor. Mater.* 73 (2004) 81;
(b) L. Alaerts, E. Séguin, H. Poelman, F. Thibault-Starzyk, P.A. Jacobs, D.E. De Vos, *Chem. Eur. J.* 12 (2006) 7353;
(c) I. Luz, F.X. Llabrés i Xamena, A. Corma, *J. Catal.* 285 (2012) 285.
- [28] H.J. Gilfoy, K.N. Robertson, T.S. Cameron, M.A.S. Aquino, *Acta Crystallogr., Sect. E* 57 (2001) m496.
- [29] (a) F.A. Cotton, C. Lin, C.A. Murillo, *PNAS* 99 (2002) 4810;
(b) T. Liworncharoenvong, R.L. Luck, *Acta Crystallogr., Sect. E* 61 (2005) m1191.
- [30] (a) E.V. Dikarev, B. Li, V.V. Chernyshev, R.V. Shpanchenko, M.A. Petrukhina, *Chem. Commun.* (2005) 3274;
(b) V.M. Miskowski, R.F. Dallinger, G.G. Christoph, D.E. Morris, G.H. Spies, W.H. Woodruff, *Inorg. Chem.* 26 (1987) 2127;
(c) G.G. Christoph, J. Halperk, G.P. Khare, Y.B. Koh, Cynthia Romanowski, *Inorg. Chem.* 20 (1981) 3029.
- [31] (a) S. Yoon, S.J. Lippard, *J. Am. Chem. Soc.* 127 (2005) 8386;
(b) M. Eddaoudi, J. Kim, D. Vodak, A. Sudik, J. Wachter, M. O'Keeffe, O.M. Yaghi, *PNAS* 99 (2002) 4900.
- [32] (a) X.-L. Wang, C. Qin, E.-B. Wang, Y.-G. Li, Z.-M. Su, L. Xu, L. Carlucci, *Angew. Chem.* 117 (2005) 5974 (*Angew. Chem., Int. Ed.* 44 (2005) 5824);
(b) Y. Gong, C.W. Hu, H. Li, K.L. Huang, W. Tang, *J. Solid State. Chem.* 178 (2005) 3152.
- [33] (a) F.A. Cotton, G.W. Rice, *Inorg. Chem.* 17 (1978) 2004;
(b) F.A. Cotton, T.R. Felthouse, *Inorg. Chem.* 19 (1980) 328.
- [34] (a) H. Li, M. Eddaoudi, T.L. Groy, O.M. Yaghi, *J. Am. Chem. Soc.* 120 (1998) 8571;
(b) F. Demirhan, J. Gun, O. Lev, A. Modestov, R. Poli, P. Richard, *J. Chem. Soc., Dalton Trans.* (2002) 2109.
- [35] A.P. Sattelberger, K.W. McLaughlin, *J. Am. Chem. Soc.* 103 (1981) 2880.
- [36] T.A. Stephenson, D.A. Tocher, M.D. Walkinshaw, *J. Organomet. Chem.* 232 (1982) c51.
- [37] T. Allman, R.C. Goel, N.K. Jha, A.L. Beauchamp, *Inorg. Chem.* 23 (1984) 914.
- [38] E.V. Dikarev, B. Li, *Inorg. Chem.* 43 (2004) 3461.
- [39] E.V. Dikarev, B. Li, H. Zhang, *J. Am. Chem. Soc.* 128 (2006) 2814.
- [40] T.G. Appleton, K.A. Byriel, J.R. Hall, C.H.L. Kennard, M.T. Mathieson, *J. Am. Chem. Soc.* 114 (1992) 7301.
- [41] K. Knabel, I. Krossing, H. Nöth, H. Schwenk-Kircher, M. Schmidt-Amelunxen, T. Seifert, *Eur. J. Inorg. Chem.* (1998) 1095.
- [42] W. Uhl, R. Graupner, S. Pohl, W. Saak, W. Hiller, M. Neumayer, *Z. Anorg. Allg. Chem.* 623 (1997) 883.
- [43] N.Yu. Kozitsyna, S.E. Nefedov, F.M. Dolgushin, N.V. Cherkashina, M.N. Vargaftik, I.I. Moiseev, *Inorg. Chim. Acta.* 359 (2006) 2072.
- [44] S. Matsunaga, K. Hasada, K. Sugiura, N. Kitamura, Y. Kudo, N. Endo, W. Mori, *Bull. Chem. Soc. Jpn.* 85 (2012) 433.
- [45] P.M. Barron, H.-T. Son, C. Hu, W. Choe, *Cryst. Growth Des.* 9 (2009) 1960.
- [46] W.W. Lestari, H. Zaake-Hertling, P. Lönnecke, E. Hey-Hawkins, *Z. Anorg. Allg. Chem.* 639 (2013) 2589.
- [47] CrysAlis Pro, Data Collection and Data Reduction Software Package Including SCALE3 ABSPACK for Empirical Absorption Correction using Spherical Harmonics, version 1.171.35.21, release 20–01-2012 CrysAlis171.NET, Agilent Technologies.
- [48] A. Altomare, G. Cascarano, C. Giacovazzo, A. Guagliardi, *J. Appl. Crystallogr.* 27 (1994) 435.
- [49] G.M. Sheldrick, *Acta Crystallogr., Sect. A* 64 (2008) 112.
- [50] SQUEEZE, P. van der Sluis, A.L. Spek, *Acta Cryst. A* 46 (1990) 194.
- [51] H. Borrmann, I. Persson, M. Sandström, C.M.V. Stålhandske, *J. Chem. Soc., Perkin Trans. 2* (2000) 393.
- [52] Diamond, Version 3.2i, Klaus Brandenburg, Crystal Impact GbR, Bonn, Germany.
- [53] V.A. Blatov, TOPOS 4.0, IUCr CompComm Newsletter. 7 (2006) 4, <http://www.topos.ssu.samara.ru>.
- [54] M. O'Keeffe, M.A. Peskov, S.J. Ramsden, O.M. Yaghi, *Acc. Chem. Res.* 41 (2008) 1782.
- [55] A.L. Spek, *PLATON*, *Acta Crystallogr., Sect. D* 65 (2009) 148.
- [56] (a) S. Asbrink, L.J. Norrby, *Acta Crystallogr., Sect. B* 26 (1970) 8;
(b) G. Tunell, E. Posnjak, C.J. Ksanda, *Z. Kristallogr.* 90 (1935) 120.
- [57] O. Kahn, *Molecular Magnetism*, VCH, New York, 1993.
- [58] R.T. Azuah, L.R. Kneller, Y. Qiu, P.L.W. Tregenna-Piggott, C.M. Brown, J.R.D. Copley, R.M. Dimeo, *J. Res. Natl. Inst. Stand. Technol.* 114 (2009) 341.
- [59] R.L. Carlin, *Magnetochemistry*, Springer, Berlin, 1986, p. 12.
- [60] (a) W. Mori, F. Inoue, K. Yoshida, H. Nakayama, S. Takamizawa, M. Kishita, *Chem. Lett.* (1997) 1219;
(b) S.C. Manna, J. Ribas, E. Zangrando, N.R. Chaudhuri, *Inorg. Chim. Acta* 360 (2007) 2589;
(c) X.Z. Wang, D.R. Zhu, Y. Xu, J. Yang, X. Shen, J. Zhou, N. Fei, X.K. Ke, L.M. Peng, *Cryst. Growth Des.* 10 (2010) 887.
- [61] A.B.P. Lever, *Inorganic Electronic Spectroscopy*, Elsevier, Amsterdam, 1984.
- [62] W.W. Lestari, P. Lönnecke, H.C. Streit, C. Wickleder, E. Hey-Hawkins, *Dalton Trans.* 43 (2014) 8188.
- [63] Y.-W. Li, J.-R. Li, L.-F. Wang, B.-Y. Zhou, Q. Chena, X.-H. Bu, *J. Mater. Chem. A* 1 (2013) 495.
- [64] W.W. Lestari, P. Lönnecke, M.B. Sárosi, H.C. Streit, M. Adlung, C. Wickleder, M. Handke, W.D. Einicke, R. Gläser, E. Hey-Hawkins, *CrystEngComm* 15 (2013) 3874.
- [65] W.W. Lestari, P. Lönnecke, H.C. Streit, M. Handke, C. Wickleder, E. Hey-Hawkins, *Eur. J. Inorg. Chem.* (2014) 1775.